Electron Transfer Reactions in LDI and MALDI: Factors Influencing Matrix and Analyte Ion Intensities

Andrew J. Hoteling[a]*, William F. Nichols[a] David J. Giesen[a] Jerome R. Lenhard[a] and Richard Knochenmuss[b]*

a) Research & Development
Eastman Kodak Company
Rochester, NY 14650-2132, USA
b) Novartis Institutes for Biomedical Research
4056 Basel, Switzerland

Author's final submitted manuscript
Published as Eur. J. Mass Spectrom., vol. 12, pp. 345-358 (2006)
DOI: 10.1255/ejms.820
URL: http://dx.doi.org/10.1255/ejms.820

Abstract

Certain analytes appear in LDI or MALDI mass spectra as radical ions, rather than deprotonated, protonated or cationized molecules. Radical ion intensity ratios are found to be consistent with matrix-analyte and analyte-analyte electron transfer (ET) reactions in the desorption/ablation plume. As predicted by the two-step model of UV-MALDI, both suppression of matrix by analytes, and one analyte by another are observed. The dependence of these effects on mixing ratios, laser fluence and matrix choice parallel suppression phenomena previously observed with proton or cation transfer reactions. The driving force for ET, as reflected in differences of gas-phase molecular ionization potentials (IPs) or solution oxidation potentials (Eox), is usually the dominant factor determining relative ion intensitites. In positive polarity, low IP (Eox) analytes suppress signals of high IP (Eox) analytes. However, for large IP (Eox) differences and at high matrx-to-analyte mole ratios, relative intensities were found to invert. This is tentatively ascribed to a rollover in the rate of matrix-analyte electron transfer at high exoergicity.

* Corresponding authors.

Introduction

Protonated or deprotonated molecular ions are frequently observed in MALDI mass spectra. In postive polarity, cationized molecules are sometimes also important, or even the dominant ions, if the analytes have low proton affinity. However, radical ions are also observed, particularly of low polarity species with few functional groups.[1-6] Although initial work did not unambiguously identify the role of the matrix,[1] it later became clear that electron transfer (ET) from neutral analytes to matrix ions is the key step in the generation of radical analyte cations.[2, 3] Directly comparable to atmospheric pressure chemical ionization with transfer reagents such as benzene, the difference in ionization potentials (IPs) of matrix and analyte or between analytes was proposed as the relevant thermodynamic parameter explaining the features of the mass spectra.[3] An analagous picture has been demonstrated for generation of radical anions of fullerene derivatives in LDI and MALDI.[4, 7] In negative polarity it is the difference in electron affinities which determines the extent of analyte ionization. It was also shown that the ET excess energy is strongly correlated with fragmentation of fluorofullerenes.[4]

The electron transfer (ET) LDI and MALDI data are consistent with the general 2-step model of UV-MALDI ionization.[8-10] In that model the laser generates primary matrix ions, which react in the expanding plume with matrix and analyte neutrals to generate secondary analyte ions. Because the plume is hot and dense for a significant time, such reactions are believed to yield the thermodynamically most favorable final ion distribution. If information is available regarding ion-molecule reaction parameters, the model can be made quantitative and predictive.[10]

The model predictions are not dependent on the nature of the ions involved, only the ion-molecule reaction thermodynamics and kinetics. Since interconversion between ion types may often be facile,[8] electron, proton and cation transfer may all be active in a single MALDI event. Proton and cation transfer energetics have been well studied from the MALDI viewpoint, and the model has been widely successful for these cases.[11-26] ET-MALDI has not previously been shown to exhibit all the phenomena predicted.

Striking MALDI effects predicted by the model, and indicators for it, are the matrix and analyte suppression effects.[4, 8, 27-31] If sufficient analyte is present, and the reaction with primary matrix ions favorable, all primary ions may be consumed. The mass spectra exhibit only analyte signals, no matrix ions are observed. This is the matrix suppression effect (MSE), which is not only intrinsically interesting, but can be put to practical use in

small molecule analysis.[32]

If multiple analytes are present, they will also react in a similar manner, with the consequence that signal ratios vary with matrix to analyte ratio. It is even possible for one analyte to fully suppress another.[8, 25] Both the analyte suppression effect (ASE) and the MSE are dependent on the number of primary ions available, and the reaction time available in the plume. As a result they can be modulated to a certain extent by the laser pulse energy. A stronger pulse generates both more primary ions and a denser plume. The former reduces suppression, the latter enhances it, if reaction kinetics are not a limitation. Neither MSE nor ASE have been systematically studied in ET-MALDI, although some ASE effects have been noted.[4]

Here we explore characteristics of ET-MALDI to understand the factors that govern ion intensities in the mass spectra of simple and complex mixtures. Motivation and a range of test cases are provided by organic light emitting diode (OLED) materials, for which reliable and predictible analytical methods are increasingly needed. Particular attention is devoted to evaluating the validity of the two-step MALDI model, since it provides a rational framework for interpretation and design of experiments. The diagnostic indicators of the model are observed, and the spectra can be rationalized in terms of gas-phase ionization potential differences, as well as with solution-phase oxidation potentials.

Experimental and Theoretical Me*thods*

Ionization Potential Calculations

Vacuum ionization potentials were calculated using Gaussian03.[33] Neutral molecules were optimized with the B3LYP[34, 35]/MIDI![36] basis, after which the difference between the B3LYP/6-31G*[36-38] neutral and unrestricted ion energies was calculated at this geometry. Several other less or more computationally intensive methods were also tested for the calculation of ionization potentials, but the method presented here gave results as good or better than the other methods. A discussion of these issues is given in the Appendix.

Oxidation Potential Measurements

Oxidation potentials (Eox) were measured by cyclic voltammetry at a scan rate of 0.1V/s using a Princeton Applied Research Corp Model 373 potentiostat/galvanostat. Solutions for voltammetry were prepared in CH_3CN/toluene (1:1) mixture containing 0.1 M tetrabutylammonium tetrafluoroborate and 1mM analyte. A two-compartment, three-electrode voltammetry cell equipped with a platinum disk working electrode and a NaCl-

saturated calomel reference electrode (SCE) at 22 °C. Ferrocene was used as an internal standard to correct data for reference electrode junction potentials. For the analyte compounds A-E the Eox were take as the average of the anodic and cathodic peaks of the reversible electrode process. The matrix materials undergo completely irreversible oxidation, hence voltammetric peak potentials were used to estimate the Eox.

MALDI Mass Spectra

Materials. The matrix materials nicotinic acid (NA), 2,5-dihydroxybenzoic acid (DHB), 1,8,9-anthracenetriol (dithranol), and 2-((2E)-3-(4-tert-butylphenyl)-2-methylprop-enylidene)malanonitrile (DCTB) were purchased from Aldrich Chemical Co. (Milwaukee, WI). The analytes (structures shown in Figure 1) were obtained from Eastman Kodak Company (Rochester, NY).

Figure 1

MALD/I Sample Preparation. Analyte samples for MALD/I and LD/I analysis were prepared at a concentration of 0.8 mM in THF. The matrix solutions were prepared at a concentration of 40 mM in THF. The samples were prepared by mixing the analyte solution with matrix solution at a volume ratio of 1:9, resulting the desired matrix:analyte mole ratio. A volume 0.5 uL of the mixture was deposited on a sample plate and allowed to air-dry. To prepare the range of M/A ratios, the matrix solution concentration was held constant and the analyte solution was diluted to achieve the desired mole ratio.

MALD/I TOFMS Instrumentation. MALDI-TOFMS experiments were carried out using a TofSpec2E laser time-of-flight (TOF) mass spectrometer (Micromass, Inc., Manchester, UK), equipped with dual microchannel plate detectors for both linear and reflectron modes and a nitrogen laser operating at 337 nm. Positive ion mode was utilized for all analyses, with an accelerating voltage of 20 kV for reflectron mode. Spectra were acquired using delayed extraction with a 500 ns delay time.

Results and Discussion

Matrix and Analyte Ionization Potentials

Experimental and calculated ionization potentials of some UV-MALDI matrices, the analytes used here and related molecules are collected in Table 1. See the Appendix for a detailed discussion of computational methods and results.

The initial comparison of the raw computed B3LYP/6-31G*//B3LYP/MIDI! IP values with experiment showed a high correlation but a slope and intercept that differed from the ideal

values of 1 and 0, respectively. Thus, it was decided to use a linear regression to obtain slope and intercept values that would convert the raw computed IP values to quantitatively agree with the known experimental values. The resulting equation is:

Corrected IP = (Raw computed IP) * 0.852 + 1.56

and the data obtained from this equation are shown in Table 1.

Table 1

The standard Eox of the analytes used in this study and some common matrixes are also listed in Table 1. As this corresponds to ionization in solution, a strong correlation with the gas phase ionization potentials might be expected and is indeed found between the computed IP and the experimental Eox values, as is shown in Figure 2.

Figure 2

Two matrix compounds show an unusual IP versus Eox relationship. Dithranol, 1,8,9-anthracenetriol, has a IP much lower than would be expected based on a plot of computed IP versus Eox. However, B3LYP/6-31G*//B3LYP/MIDI! calculations find the ketone tautomer, 1,8-dihydroxyanthrone, to be more stable by 20 kcal/mol. Infrared and NMR spectroscopy in both solid and solution phases support this conclusion. Thus, Table 1 also gives data for this tautomer of dithranol, showing that the computed IP for this tautomer fits nicely with the experimental Eox data. Other than dithranol, the only mismatch between computed IP and Eox data is 2,5-dihyrdoxybenzoic acid (2,5 DHB), and given the good agreement between computed and experimental IP for this and other benzoic acid compounds, it is likely that the IP/Eox disparity lies either in condensed phase effects on the Eox measurement or in problems with the measurement of the irreversible oxidation. Figure 2 plots the computed IP versus experimental Eox, using the data for 1,8-dihydroxyanthone. Without the data for 2,5-dihydroxybenzoic acid, the R^2 between computed IP and experimental Eox for the remaining 8 compounds is 0.984.

LDI and MALDI of OLED Analyte Mixtures

General Characteristics of ET MALDI Figure 3 shows LDI and MALDI positive ion mass spectra of a 5 component mixture of OLED compounds. In both cases, only radical cations are observed.

Since all of the analytes are readily observed by LDI and 2 laser photons are sufficient to

ionize all analytes, a direct photoionization mechanism is likely to be active. Analytes D and E were found have little to no absorbance at 337 nm, while the other three have strong absorbance at 337 nm (data not shown). Presumably the absorbing analytes generate the primary ions in LDI, with subsequent charge transfer to the non-absorbing analytes. This is supported by the similar LDI responses for analytes C and D, even though their absorbances at 337 nm are dramatically different. Analytes A, B and C are effectively acting as MALDI matrices for analytes D and E.

In the conventional MALDI experiment where the analytes are present at low concentration in DCTB matrix, direct analyte photoionization of the absorbing analytes is undoubtedly occuring, but does not play a dominant role. If this were the case, signals of analytes A, B and C would each be independent, and no suppression effects involving them would be observed. As is clear in Figs. 3 and 4, suppression is occurring. This is a consequence of the excess of matrix, which generates most ions. Secondary ionization of analyte by matrix is far more likely than direct ionization of analyte. It has been shown that very high analyte concentrations are needed to generate a significant number of ions via direct photoionization.[39]

Relative intensities in Figs. 3 and 4 are much better correlated with oxidation and ionization potentials than with absorption of the laser wavelength. The substances with the highest oxidation potentials and (method 4 fit) IPs give the smallest signals. All analyte IPs are below that of the DCTB matrix, and all species are observed as radical cations.

Figure 3

By analogy to the earlier studies noted above, Fig. 3 suggests that the mass spectra are determined by the reactions below, taking place in the expansion plume:

$$M^{+\bullet} + A \rightarrow M + A^{+\bullet} \quad (1)$$

$$A^{+\bullet} + B \rightarrow A + B^{+\bullet} \quad (2)$$

Where M = matrix, A = analyte, and B = second analyte. As written, reaction 1 is favorable if the ionization potential of M is greater than that of A. Similarly, reaction 2 is favorable if the ionization potential of A is greater than that of B. Low IP analyte ions are therefore favored, either by preferential depletion of high IP primary matrix ions or by reaction with

high IP analyte ions.

The reaction free energies determine the extent of secondary analyte ion formation. For many ion-molecule reactions, the reaction kinetics will also be correlated with the net free energy change,[10] so a more favorable reaction will also be faster. The relevant free energy is that of gas-phase reactions. This is true even if considerable reaction is expected in the sample prior to desorption/ablation or in clusters further downstream.[25] This is because binary collisions are the last events that every ion will experience in the thinning plume. These final gas-phase reactions determine the distribution of ions observed at the detector. Nevertheless, a clear correlation is also observed between the ion signals and solution phase oxidation potentials, as generally expected.

If this picture is correct, it should be possible to observe matrix and analyte suppression effects (MSE and ASE) analagous to those which are well established for protonation, deprotonation and cationization reactions.[30, 31] The MSE and ASE are concentration dependent, since enough analyte must be present to consume all primary matrix ions. Often, M/A ratios of 500 or less are needed for MSE when protonation or deprotonation reactions are involved.[10, 30] As shown in Fig. 4 for the same 5 component mixture with DCTB matrix, MSE is observed in ET MALDI, and is concentration dependent. The M/A ratio at which it appears can be remarkably high. This is not observed in every case, even with this matrix. However, M/A ratios for suppression of 1000 or higher were often found, which may have important implications for a detailed model. A possible reason for this is the greater range of ET vs. proton or cation transfer, especially when via conjugated pi-systems such as are found in both matrices and analytes.

Figure 4

Coincident with the appearance of MSE is the relative enhancement of low IP substances, which is particularly evident if the normalized signals are plotted vs. M/A ratio as in Fig. 5. At the highest ratios, analyte signals should reflect an "intrinsic," or limiting sensitivity (ion signal/concentration in the sample) for each individual analyte, since primary ions are in excess and reaction 2 is unimportant. In this mixture D2NA (analyte E) yields relatively low signal at high M/A, for example. As more analyte is added, MSE develops and low IP analytes become increasingly favored.

Figure 5

At the higher analyte concentrations, inter-analyte ET reactions (reaction 2) become more significant, further suppressing high IP substances in favor of those with low IP. This can lead to complete suppression of one analyte by another (ASE), as demonstrated in Fig. 6. Note that ASE is accompanied, and usually preceeded, by MSE. Again, this effect has a well-established counterpart in MALDI of protonating, deprotonating and cationizing analytes.

Figure 6

In both the MSE and ASE, the quantity of primary matrix ions plays a key role, by limiting the extent of reaction 1. Obviously, if more matrix ions than neutral analyte are present, then matrix suppression cannot occur. In the ASE, the quantity of matrix ions determines the quantity of secondary A^+ ions that can be involved in reaction 2. Since M^+ populations depend on the laser intensity, this easily adjusted parameter can help evaluate the applicability of the model. Strong MSE or ASE at low laser intensities should decrease at high intensities.[10, 30] This may also be analytically useful, to obtain more correct signal ratios, although the quality of the mass spectrum may decrease due to the very dense plume. The laser dependence of ET MSE and ASE is shown in Fig. 7.

Figure 7

At low intensities, full MSE is observed, as is the now familiar relative suppression of high IP analytes. As the laser becomes more intense, analyte ratios exhibit less suppression, although equal signals for all analytes are not obtained. Because of broadening, peak areas should be compared, rather than peak heights, as shown in the bar graph of Fig. 8. At the highest intensities, matrix signals reappear and primary ions are no longer completely consumed.

Figure 8

Energetics of ET MALDI While a general preference for low-IP (or oxidation potential) analytes was shown in the 5-component sample above, binary mixtures provide a means to investigate the energetics of ET MALDI more closely. Of particular interest are the differences in IP between matrix and analytes and between the analytes themselves. The most important difference is that between matrix and analyte. While many matrices are

small molecules with relatively high IPs, this is not always the case. If the IP of the matrix is not higher than that of an analyte, no signal should be observed. Figure 9 shows a possible example of this with the binary mixture of analytes D and E, and dithranol as the matrix.

Figure 9

Essentially no analyte E signal is observed. Since the IP of E (est=7.06 eV) is near or above that of the matrix dithranol (est=6.94 eV) this would be consistent with reaction 1. (The very small signals at the lowest M/A ratios could be due to direct absorption of the laser by analyte E.) The IP of D lies lower (est=6.50 eV), and it is readily observed, as expected. This interpretation must be treated carefully, however, since NMR spectra of dithranol in a variety of solvents and solvent mixtures, and infrared spectroscopy of the solid found only the 1,8-dihydroxyanthrone isomer, which has an estimated IP of 8.17 eV. whether it reverts to the trihydroxy form in the gas phase remains unknown.

Figure 6 demonstrated suppression of analyte D (IP est.=6.50 eV, Eox=0.884 V) by analyte A (IP est.=6.04 eV, Eox=0.423 V). Figure 10 shows that analyte E (IP est.=7.06 eV, Eox=1.273 V) can in turn be suppressed by analyte D. The matrix DCTB (IP est.=8.22 eV, Eox=ca. 2.1) is suppressed in both cases. Several other binary combinations have been investigated with similar results.

Figure 10

While both examples are consistent with the MALD/I model, Fig. 6 exhibits somewhat more vigorous suppression. Both MSE and ASE appear at higher M/A ratios. For MSE, this is a reflection of the considerably larger driving force (IP or redox differences) for reaction 1 with A than with E. The ASE trend is correlated with the analyte IP differences and redox potential differences as well. In Figure 6, the differences are: IP: 0.46 eV, redox: 0.461 V. In Figure 10 these are 0.56 eV and 0.389 V, respectively. In addition to IP values, oxidation potentials appear to be relevant for ET-MALDI prediction and interpretation. This may reflect a relatively solution-like environment for charge transfer, if reactions 1 and 2 take place to a large extent in the dense region of the expansion plume.

It is useful to compare the energetics of electron transfer in MALDI with those of more common protonation and cationization reactions. In combination with popular matrices,

protonation of proteins and peptides is quite favorable, with a net exothermicity often well over 100 kJ/mol (1 eV = 96.5 kJ/mol).[10] Cationization is much less energetic, so it tends to be important only for analytes of low basicity, such as many synthetic polymers. Cationization with Na+ has a net exothermicity on the order of 20-50 kJ/mol (or 0.2-0.5 eV) for common matrices and analytes.[10] The nonlinear free energy relationship of Agmon and Levine[40] used to estimate the rates of ion transfer reactions predicts that typical proton transfers will be fast, leading to facile matrix suppression, as observed. Cation transfers can be kinetically limited, but are often not.

ET reactions can be very exothermic. Gas phase IP differences between matrix and analyte in this study are up to 3 eV. This is largely reflective of the analytes involved, which have extended aromatic pi-electron systems, and consequently low IPs. At the same time their proton affinities are relatively low. The proton affinity of benzene is 7.77 eV, 1 eV below that of typical matrices.[11, 12, 14-17, 41] For these analytes the outcome of a MALDI experiment is clear: an endothermic proton transfer cannot compete with a highly exothermic electron transfer.

Kinetics of ET MALDI IP differences are the driving force for electron transfer. If the IP difference between matrix and analyte (or between analytes) increases, reactions 1 and 2 should shift further toward the products, modifying the appropriate ion signals in the mass spectrum. This will be the case as long as the reactions have sufficient time to approach equilibrium. If either reaction is slow compared to the plume expansion to collision-free conditions, kinetic limitations on the relative ion yields may appear. For proton and cation transfer reactions no kinetic limitations were observed except when free energy changes were quite small or the laser intensity was very low. This is a consequence of the relatively low activation barriers for favorable ion transfer reactions as noted above.

In MALDI electron transfer ionization, however, kinetic effects are apparently active. As shown in Fig. 11, very low IP analytes are unexpectedly weak in combination with high IP matrices, at high M/A ratio. Analytes D and E have the expected relative intensities at lower M/A, but invert at very high M/A. The same effect is found in Fig. 6, where analytes A and D invert. The M/A ratio is important, since a high dilution means that few inter-analyte reactions are modifying the relative A^+:B^+ intensities resulting from isolated reaction of each analyte with matrix. As a result we see the relative intensities due to reaction 1, without 2. That the same analyte pairs give the expected result with other matrices of lower IP strongly suggests that a kinetic limitation is operative at high IP difference.

Figure 11

Inversion at high M/A ratio was only observed when a large IP or Eox difference exists between matrix and the inverting analyte. A threshold energy difference for inversion in ET MALDI may exist, as can be seen for the 5-component mixture in Figs. 3 and 4. It appears that inversion first occurs near the energy difference between DCTB and analyte C, or 1.5 eV. At the highest dilutions, analytes with IPs lower than that of analyte C decrease in relative intensity.

Conclusions

The characteristics of LDI and MALDI were investigated for analytes used in OLEDs. Ion-molecule electron transfer reactions lead to a general relative suppression of higher IP/oxidation potential analytes in positive polarity. In both MALDI and LDI, such suppression effects were found to be very significant, but MALDI offers more potential to modulate or moderate them, via matrix choice and M/A ratio.

In MALDI, MSE and ASE were found at M/A ratios higher than needed for suppression based on proton transfer reactions. Still higher M/A ratios reduced the suppression effects, but ion intensities never quantitatively reflected the composition of the original sample. Increased laser intensity also reduced suppression effects, but did not eliminate them.

These characteristics are indicative of and consistent with the two step model of MALDI ionization, based on the thermodynamics of plume reactions. Both *ab initio* estimates of gas-phase IPs and solution phase redox potentials were found to be useful in predicting and interpreting the mass spectra, although both also have limitations. In positive polarity, low IP (Eox) analytes generally suppress signals of high IP (Eox) analytes.

Exceptions to the above rule are observed when IP differences between matrix and analyte are large, >1.5 eV, and the M/A ratio is a high. Observed ion signal ratios can then be the opposite of what is expected from the reaction exoergicity. This is tentatively ascribed to a rollover in the rate of matrix-analyte electron transfer.

Acknowlegments

The authors would like to thank the following for their contributions to this work: Denis Y. Kondakov (Eastman Kodak Company) for discussions about electron transfer reactions, and William C. Lenhart (Eastman Kodak Company) for NMR studies of dithranol.

Appendix: Computational Methods

Calculations were performed with both the General Atomic and Molecular Electronic Structure System (GAMESS),[42] on Apple Powermac G4 and G5 desktop computers, and with Gaussian 03[33]on Beowulf cluster of Pentium IV computers.

Three methods were used to calculate vertical molecular ionization potentials (IPs) with GAMESS: 1) The Koopmans[43] approximation was used at the neutral molecule stationary point calculated using the 4-31G(d,p)[37, 44] basis. AM1[45] semi-empirical calculations were used to evaluate possible low energy conformations prior to *ab initio* optimization. 2) The neutral geometry was optimized using a 6-31+G(d,p)[37, 38, 44] basis with the B3LYP[34, 35] exchange-correlation functional. The difference between the the neutral RB3LYP and the ion ROB3LYP[46] energies at this geometry was taken as the IP. 3) The geometry of (2) was used for RB3LYP neutral and ROB3LYP calculations with a B3LYP/6-311++G(2d,p,f)[47, 48] basis. Methods (2) and (3) are the same as or very similar to those used in earlier computational studies of some MALDI matrices.[13-16]

The fourth method used Gaussian 03. The neutral molecules were optimized with the B3LYP/MIDI![36] basis, after which the difference between the B3LYP/6-31G* neutral and unrestricted ion energies was calculated at this geometry.

By default, GAMESS and Gaussian 03 use different definitions of the B3LYP method.[33, 42] The default method in both programs was used. Based on tests using the same basis set in both programs, Gaussian 03 gives B3LYP ionization potentials that are between 0.1 and 0.2 eV higher than GAMESS.

Experimental and calculated ionization potentials of some UV-MALDI matrices, the analytes used here and related molecules are collected in Table A1. All four computational methods correlate nearly equally well with experiment, but the HF Koopmans Approximation - Method 1 - is quantitatively the best. The large mean signed error of the DFT methods and equivalent R^2 values of all the methods indicate that the difference between the HF method and the DFT methods is mostly a constant offset. This is supported by the R^2 values for correlation between Method 1 and the others, which are 0.98-0.99.

These results are somewhat surprising since it is widely believed that extensive basis sets are necessary for accurate *ab initio* estimation of molecular properties. On the other hand, all methods represent implicit approximations of partially unknown and poorly predictable nature. It is therefore possible that a "low quality" basis will exhibit advantageous error cancellation characteristics for particular purposes and molecules, particularly when combined with assumptions such as Koopman's approximation.

It was found that the computed IP values had very little dependence on the basis set used for geometry optimization. When the same basis set and version of B3LYP was used to calculate the neutral and cation energies, the difference in IP between B3LYP/MIDI! geometries and B3LYP/6-31+G(d,p) geometries was typically less than 0.05 eV and never surpassed 0.10 eV. Thus, the larger basis set, along with the associated longer compute time and SCF convergence problems, is not necessary for geometry optimization.

At the same time, larger basis sets significantly affect the computed IP at a given geometry. It can be seen in Table 1 that Methods 2 and 3, which include diffuse basis functions in the energy calculation, have larger computed IP values than Method 4, which does not include diffuse functions. This is reasonable, since the diffuse functions will have the most stabilization effect on the state that has the most diffuse electron density, which is here the ground state. However, it can also be seen that the correlation with experimental IP data is just as good with the smaller basis set as with the larger, more diffuse, basis sets.

It is fortunate that Methods 1 and 4 are suitable for IP estimation, since the other methods can be difficult or time-consuming. For example, the approximate linear dependence of bases that include many polarization and diffuse functions inhibited or prevented convergence of wave functions for the larger molecules of Table 1, as well as for ion states of some smaller molecules. Even with the simple basis, stationary point location of molecules with many degrees of freedom can be very slow, particularly if multiple conformations must be compared. Adding DFT and many extra basis functions is then effectively impractical on desktop computers.

Because the methods have both high R^2 values and high mean signed errors, the agreement with experiment will be improved by a linear fit to experiment for all the compounds that have experimental data in Table 1. Only Methods 1 and 4 were fit in this manner, since Methods 2 and 3 do not offer an improvement in accuracy but do

significantly increase the computing time. These fits reduced the RMS deviation from experiment to 0.25 eV (Method 1) and 0.24 ev (Method 4):

$$\text{Estimated IP} = (\text{Method 1 IP}) * 0.867 + 1.20$$

or

$$\text{Estimated IP} = (\text{Method 4 IP}) * 0.852 + 1.56$$

Table A1

The nearly identical slopes but different intercepts of these equations again confirm that the methods differ mostly by a constant offset over the set compounds with experimental IP data. A difference is seen, however, in analytes A-E. Analytes A, B and C contain amine groups, and ionization originates primarily at the nitrogen lone pairs in these compounds. This is a functionality not seen in the training set compounds, where ionization primarily originates in the pi electrons. Table 1 shows that Method 4 finds the amine compounds to be the most easily ionized compounds in the group, and this correlates well with solution data from experimental Eox of analytes A-E, with an R^2=0.991 between the two sets of data. Method 1, on the other hand, finds these compounds relatively more difficult to ionize, in disagreement with the experimental Eox. This type of difficulty when comparing results between chemically distinct classes is common with more empirical methods such as Koopmans approximation. For this reason, results from the fit of Method 4 results were used for the discussion above.

The standard Eox of the analytes used in this study are also listed in Table 1. As this corresponds to ionization in solution, a strong correlation with the gas phase ionization potentials is expected. With method 1 this is roughly observed, but the trend is not monotonic. Method 4, on the other hand, is uniformly correlated with the Eox and is more useful for predicting or understanding ET MALDI spectra, as discussed below.

References

1. P. Juhasz, C. E. Costello, *Rapid Commun. Mass Spectrom.* **7**, 343 (1993).
2. T. D. McCarley, R. L. McCarley, P. A. Limbach, *Anal. Chem.* **70**, 4376 (1998).
3. S. F. Macha, T. D. McCarley, P. A. Limbach, *Anal. Chim. Acta* **397**, 235 (1999).
4. A. Streletskii, I. N. Ioffe, S. G. Kotsiris, M. P. Barrow, T. Drewello, S. H. Strauss, O. G. Boltalina, *J. Phys. Chem. A* **109**, 714 (2005).
5. R. Lidgard, M. W. Duncan, *Rapid Commun. Mass Spectrom.* **9**, 128 (1995).
6. L. Ulmer, J. Mattay, H. G. Torres-Garcia, H. Luftmann, *Eur. J. Mass Spectrom.* **6**, 49 (2000).
7. T. Brown, N. L. Clipston, N. Simjee, H. Luftmann, H. Hungerbuhler, T. Drewello, *Int. J. Mass Spectrom.* **210/211**, 249 (2001).
8. R. Knochenmuss, A. Stortelder, K. Breuker, R. Zenobi, *J. Mass Spectrom.* **35**, 1237 (2000).
9. R. Knochenmuss, *J. Mass Spectrom.* **37**, 867 (2002).
10. R. Knochenmuss, *Anal. Chem.* **75**, 2199 (2003).
11. M. Mormann, S. M. Bashir, P. J. Derrick, D. Kuck, *J. Am. Soc. Mass Spectrom.* **11**, 544 (2000).
12. R. D. Burton, C. H. Watson, J. R. Eyler, G. L. Lang, D. H. Powell, M. Y. Avery, *Rapid Commun. Mass Spectrom.* **11**, 443 (1997).
13. F. H. Yassin, D. S. Marynick, *J. Mol. Struct.* **629**, 223 (2003).
14. F. H. Yassin, D. S. Marynick, *Mol. Phys.* **103**, 183 (2005).
15. S. Bourcier, S. Bouchonnet, Y. Hoppilliard, *Int. J. Mass Spectrom.* **210/211**, 59 (2001).
16. S. Bourcier, Y. Hoppilliard, *Int. J. Mass Spectrom.* **217**, 231 (2002).
17. K. Breuker, R. Knochenmuss, R. Zenobi, *J. Am. Soc. Mass Spectrom.* **10**, 1111 (1999).
18. K. Breuker, R. Knochenmuss, R. Zenobi, *Int. J. Mass Spectrom.* **184**, 25 (1999).
19. D. Yao, C. Jenkins, K. Prater, G. R. Kinsel, *International Conference on Laser Probing* (2002).
20. Z. Wu, C. Fenselau, *J. Am. Soc. Mass Spectrom.* **3**, 863 (1992).
21. Z. Wu, C. Fenselau, *Tetrahedron* **49**, 9197 (1993).
22. J. Zhang, T.-K. Ha, R. Knochenmuss, R. Zenobi, *J. Phys. Chem. A* **106**, 6610 (2002).
23. J. Zhang, R. Knochenmuss, E. Stevenson, R. Zenobi, *J. Mass Spectrom.* **213**, 237 (2002).
24. R. Knochenmuss, E. Lehmann, R. Zenobi, *Eur. Mass Spectrom.* **4**, 421 (1998).
25. R. Knochenmuss, R. Zenobi, *Chem. Rev.* **103**, 441 (2003).
26. J. Zhang, R. Zenobi, *J. Mass Spectrom.* **39**, 808 (2004).
27. T.-W. D. Chan, A. W. Colburn, P. J. Derrick, *Org. Mass Spectrom.* **27**, 53 (1992).
28. T.-W. D. Chan, A. W. Colburn, P. J. Derrick, *Org. Mass Spectrom.* **26**, 342 (1991).
29. S. Metzger, PhD Mathematisch-Naturwissenschaftliche Fakultät, Heinrich-Heine-Universität, Düsseldorf (2001).
30. R. Knochenmuss, F. Dubois, M. J. Dale, R. Zenobi, *Rapid Commun. Mass Spectrom.* **10**, 871 (1996).
31. R. Knochenmuss, V. Karbach, U. Wiesli, K. Breuker, R. Zenobi, *Rapid Commun. Mass Spectrom.* **12**, 529 (1998).
32. G. McCombie, R. Knochenmuss, *Anal. Chem.* **76**, 4990 (2005).
33. M. J. Frisch, G. W. Trucks, H. B. Schlegel, G. E. Scuseria, M. A. Robb, J. R. Cheeseman, J. A. Montgomery, T. Vreven, K. N. Kudin, J. C. Burant, J. M. Millam, S. S. Iyengar, J. Tomasi, V. Barone, B. Mennucci, M. Cossi, G. Scalmani, N. Rega, G. A. Petersson, H. Nakatsuji, M. Hada, M. Ehara, K. Toyota, R. Fukuda, J. Hasegawa, M. N. Ishida, T., Y. Honda, O. Kitao, H. Nakai, M. Klene, X. Li, J. E. Knox, H. P. Hratchian, J. B. Cross, C. Adamo, J. Jaramillo, R. Gomperts, R. E. Stratmann, O. Yazyev, A. J. Austin, R. Cammi, C. Pomelli, J. W. Ochterski, P. Y. Ayala, K. Morokuma, G. A. Voth, P. Salvador, J.

J. Dannenberg, V. G. Zakrzewski, S. Dapprich, A. D. Daniels, M. C. Strain, O. Farkas, D. K. Malick, A. D. Rabuck, K. Raghavachari, J. B. Foresman, J. V. Ortiz, Q. Cui, A. G. Baboul, S. Clifford, J. Cioslowski, B. B. Stefanov, G. Liu, A. Liashenko, P. Piskorz, I. Komaromi, R. L. Martin, D. J. Fox, T. Keith, M. A. Al-Laham, C. Y. Peng, A. Nanayakkara, M. Challacombe, P. M. W. Gill, B. Johnson, W. Chen, M. W. Wong, C. Gonzalez, J. A. Pople, *Revision B.05* **Gaussian Inc. Pittsburgh PA**, (2003).
34. A. D. Becke, *Phys. Rev. A* **38**, 3098 (1968).
35. P. J. Stephens, F. J. Devlin, C. F. Chabalowski, M. J. Frisch, *J. Phys. Chem.* **98**, 11623 (1994).
36. R. E. Easton, D. J. Giesen, A. Welch, C. J. Cramer, D. G. Truhlar, *Theo. Chim. Acta.* **93**, 281 (1996).
37. P. C. Hariharan, J. A. Pople, *Theo. Chim. Acta.* **28**, 213 (1973).
38. T. Clark, J. Chandrasekhar, G. W. Spitznagel, P. v. R. Schleyer, *J. Comp. Chem.* **4**, 294 (1983).
39. R. Knochenmuss, *Anal. Chem.* **76**, 3179 (2004).
40. N. Agmon, R. D. Levine, *Israel J. Chem.* **19**, 330 (1980).
41. K. Breuker, R. Knochenmuss, J. Zhang, A. Stortelder, R. Zenobi, *Int. J. Mass Spectrom.* **226**, 211 (2003).
42. M. W. Schmidt, K. K. Baldridge, J. A. Boatz, S. T. Elbert, M. S. Gordon, J. J. Jensen, S. Koseki, N. Matsunaga, K. A. Nguyen, S. Su, T. L. Windus, M. Dupuis, J. A. Montgomery, *J. Comput. Chem.* **14**, 1347 (1993).
43. T. Koopmans, *Phys. Scr.* **1**, 104 (1933).
44. W. J. Hehre, R. Ditchfield, J. A. Pople, *J. Chem. Phys.* **56**, 2257 (1972).
45. M. J. S. Dewar, E. G. Zoebisch, E. F. Healy, J. J. P. Stewert, *J. Am. Chem. Soc.* **107**, 3902 (1985).
46. T. Bally, Borden, W. T., *Reviews in Computational Chemistry* 1 (1999).
47. R. Krishnan, J. S. Binkley, R. Seeger, J. A. Pople, *J. Chem. Phys.* **72**, 650 (1980).
48. A. D. McLean, G. S. Chandler, *J. Chem. Phys.* **72**, 5639 (1980).
49. E. P. Hunter, S. G. Lias, **NIST Chemistry Webbook, NIST Standard Reference Database Number 69**, (1998).
50. V. Karbach, R. Knochenmuss, *Rapid Commun. Mass Spectrom.* **12**, 968 (1998).

Table 1: Experimental and calculated ionization potentials (eV) and Eox (V vs. SCE). The calculated values are corrected by linear regression to the experimental data, as discussed in the Appendix.

	Method		
Compound	Expt	Calc	Eox
Analyte A		6.04	0.423[e]
			0.707
Analyte B		6.28	0.728[e]
			0.907
Analyte C		6.45	0.820[e]
			1.009
Analyte D	6.41[a]	6.50	0.884
dithranol		6.94	ca. 2.1
Analyte E		7.06	1.273
retinoic acid		7.09	
anthracene	7.43[a]	7.41	1.33[d]
sinapinic acid		7.72	
IAA		7.75	
5-MeO SA	8.24[c]	8.09	
1,8-dihydroxyanthrone		8.17	ca. 2.1
2,5 DHB	8.054[b]	8.19	1.20[d]
DCTB		8.22	ca. 2.1
HABA		8.32	
2,3 DHB	8.249[c]	8.37	
THAP		8.44	
5-Me SA	8.24[c]	8.47	
CHCA		8.50	
SA		8.67	
3-OH BA	9.2[a]	8.78	
4-OH BA	9.2[a]	8.83	

BA	9.3[a]	9.43
nicotinic acid	9.38[a]	9.63
R^2 vs. experiment	0.94	
Mean signed error	0.00	
RMS error	0.23	

Notes: IAA= indole acrylic acid, SA = salicyclic acid, MeO = methoxy, Me = methyl, DHB = dihydroxybenzoic acid, HABA = (4-hydroxyphenolazo) benzoic acid, CHCA = alpha-hydroxy cyanocinnamic acid, THAP = trihydroxy acetophenone, BA = benzoic acid. a) NIST Webbook[49] b) Ref. 50 c) Measured in the same manner as in Ref. 50, but not previously reported. d) irreversible e) 2 reversible waves

Table A1: Calculated and experimental ionization potentials (in eV) of several MALDI matrices, the analytes used here and related molecules. The columns 1 fit and 4 fit are the data of methods 1 and 4 after a linear regression fit to the experimental values. The Eox of some analytes are also shown (in V vs. SCE).

		Method						
Compound	Expt	1	1 fit	2	3	4	4 fit	Eox
Analyte A		6.15	6.53			5.26	6.04	0.423[e]
								0.707
Analyte B		6.59	6.91			5.55	6.28	0.728[e]
								0.907
Analyte C		6.81	7.10			5.74	6.45	0.820[e]
								1.009
Analyte D	6.41[a]	6.22	6.59	6.03		5.80	6.50	0.884
dithranol		6.54	6.87	6.54	6.57	6.32	6.94	ca. 2.1
Analyte E		6.84	7.13	6.62		6.46	7.06	1.273
retinoic acid		7.57	7.76	6.81	6.85	6.50	7.09	
anthracene	7.43[a]	6.97	7.24	7.05	7.09	6.88	7.41	1.33[d]
sinapinic acid		7.80	7.96	7.46	7.49	7.24	7.72	
IAA		7.61	7.80	7.49	7.53	7.27	7.75	
5-MeO SA	8.24[c]	8.02	8.15	7.82	7.83	7.67	8.09	
1,8-dihydroxyanthrone						7.76	8.17	ca. 2.1
2,5 DHB	8.054[b]	8.12	8.24	8.04	8.05	7.79	8.19	1.20[d]
DCTB		8.36	8.45	7.92		7.82	8.22	ca. 2.1
HABA		8.13	8.25	7.67	7.69	7.93	8.32	
2,3 DHB	8.249[c]	8.26	8.36	8.15	8.16	7.99	8.37	
THAP		8.66	8.71	8.21	8.21	8.08	8.44	
5-Me SA	8.24[c]	8.38	8.47	8.27	8.28	8.12	8.47	
CHCA		8.62	8.67	8.37	8.39	8.15	8.50	
SA		8.65	8.70	8.60	8.62	8.35	8.67	
3-OH BA	9.2[a]	8.72	8.76	8.70	8.71	8.48	8.78	
4-OH BA	9.2[a]	8.85	8.87	8.75	8.78	8.53	8.83	
BA	9.3[a]	9.34	9.30			9.25	9.43	
nicotinic acid	9.38[a]	9.81	9.71	9.62		9.47	9.63	
R^2 vs. experiment		0.93	0.93	0.94	0.88	0.94	0.94	
Mean Signed Error		-0.10	0.00	-0.21	-0.24	-0.37	0.00	
RMS Error		0.29	0.24	0.33	0.32	0.46	0.23	

Notes: For compound abbreviations see Table 1 Notes. a) NIST Webbook[49] b) Ref. 50 c) Measured in the same manner as in Ref. 50, but not previously reported. d) irreversible.e) 2 reversible waves

Figures

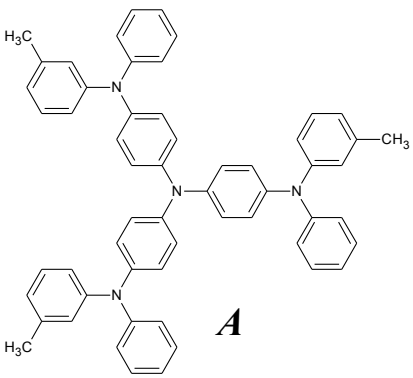

A

CAS#: 124729-98-2
Monoisotopic mass: 788.4

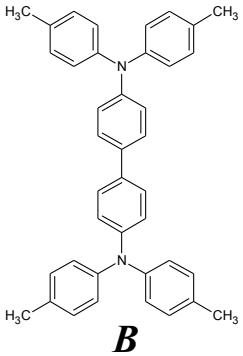

B

CAS#: 76185-65-4
Monoisotopic mass: 544.3

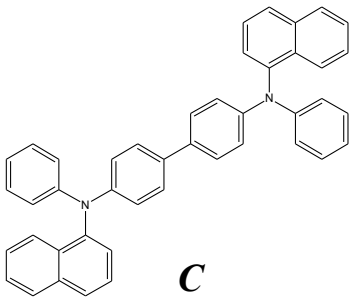

C

CAS#: 123847-85-8
Monoisotopic mass: 588.3

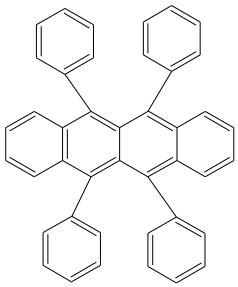

D

CAS#: 104751-29-9
Monoisotopic mass: 532.2

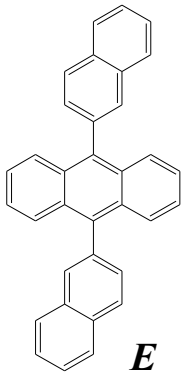

E

CAS#: 122648-99-1
Monoisotopic mass: 430.2

Figure 1. Structures of the analytes investigated. A= M-Tdata (CAS number: 124729-98-2), B= TTB (76185-65-4), C=NPB (123847-85-8), D=rubrene (104751-29-9), E=D2NA (122648-99-1).

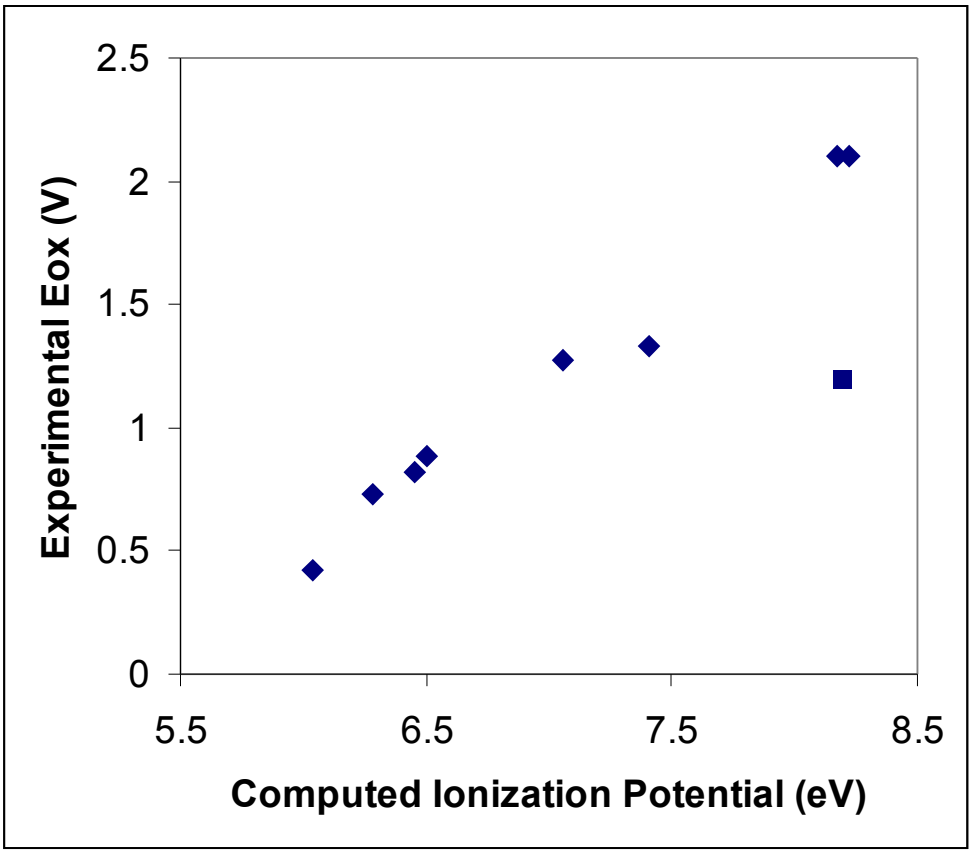

Figure 2. Plot of computed IP versus experimental Eox for the nine compounds in Table 1 with experimental Eox data. The data for 2,5-dihydroxybenzoic acid is plotted as a square.

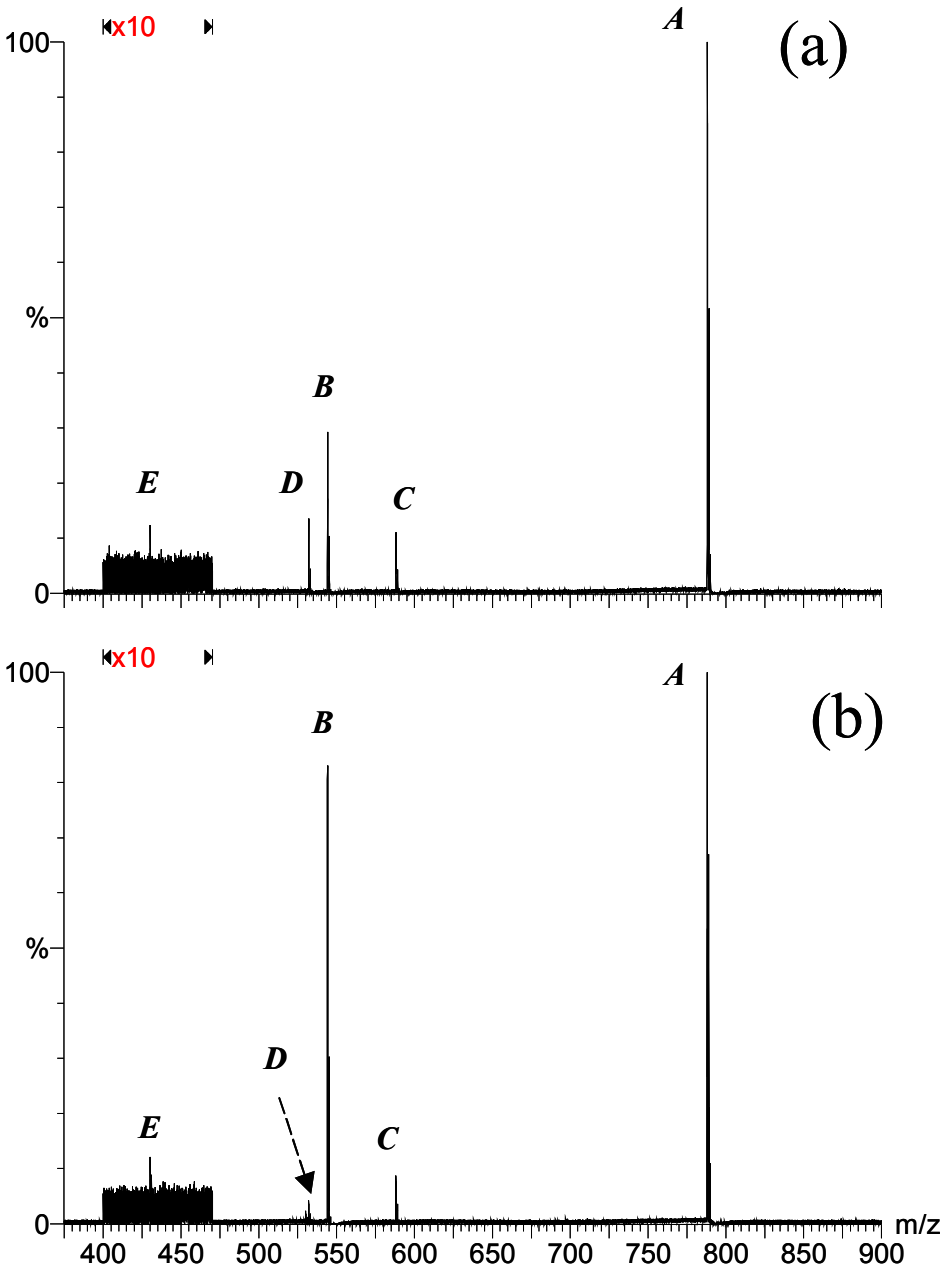

Figure 3. Five-component mixture covering a range of IPs/oxidation potentials: (a) MALDI using DCTB as the matrix with a matrix/analyte molar ratio of 500, and (b) LDI using a thin film from THF solution. The region of the spectra around m/z 430 has been expanded by a factor of 10. (See Figure 1 for analyte structures).

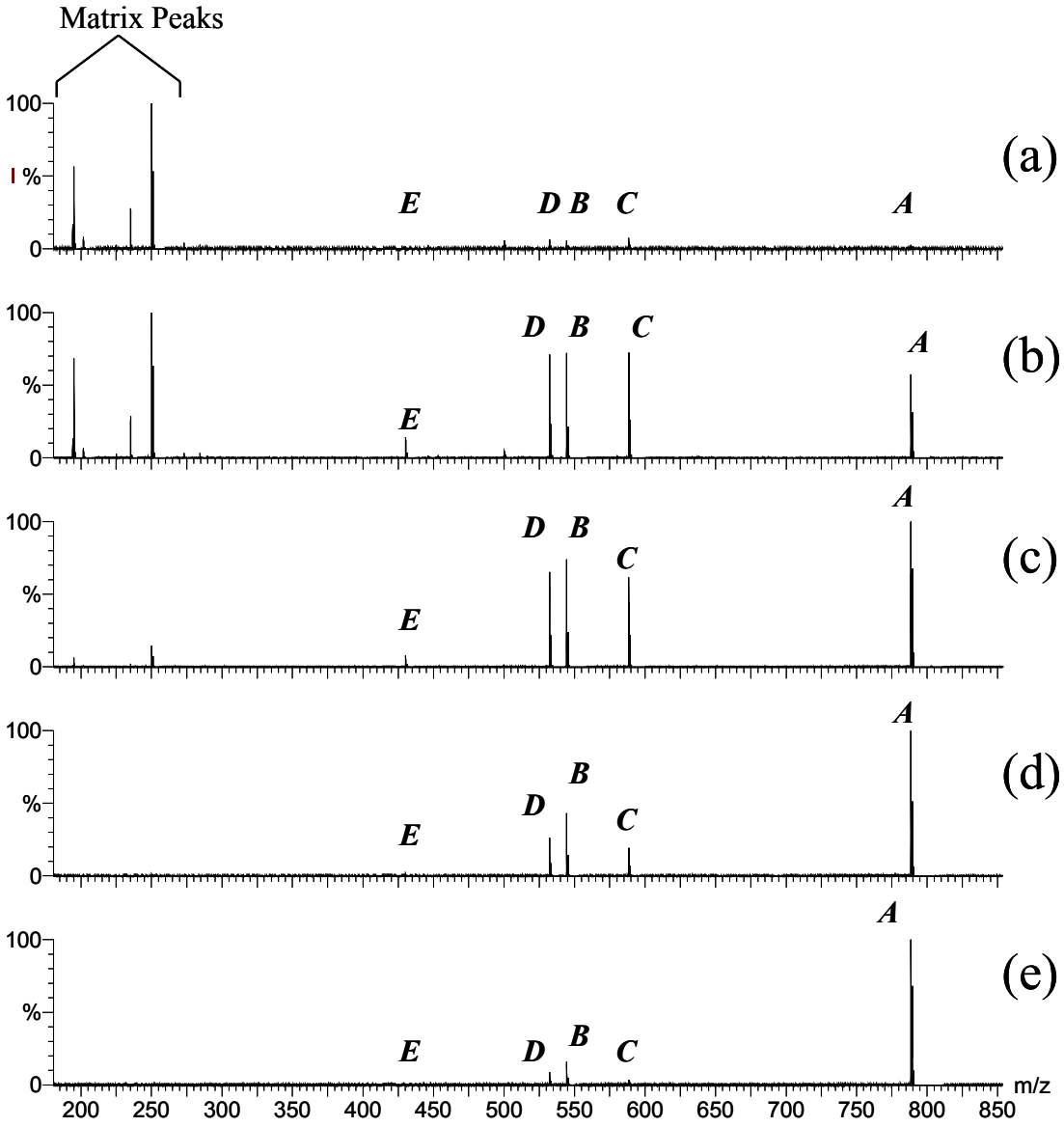

Figure 4. MALDI of equimolar five-component mixture using DCTB as the matrix, over a range of matrx to analyte mole ratios. Note the suppression of matrix when sufficient analyte is present. a) M/A=690000, b) 69000, c) 6900, d) 690, and e) 77. (See Figure 1 for analyte structures)

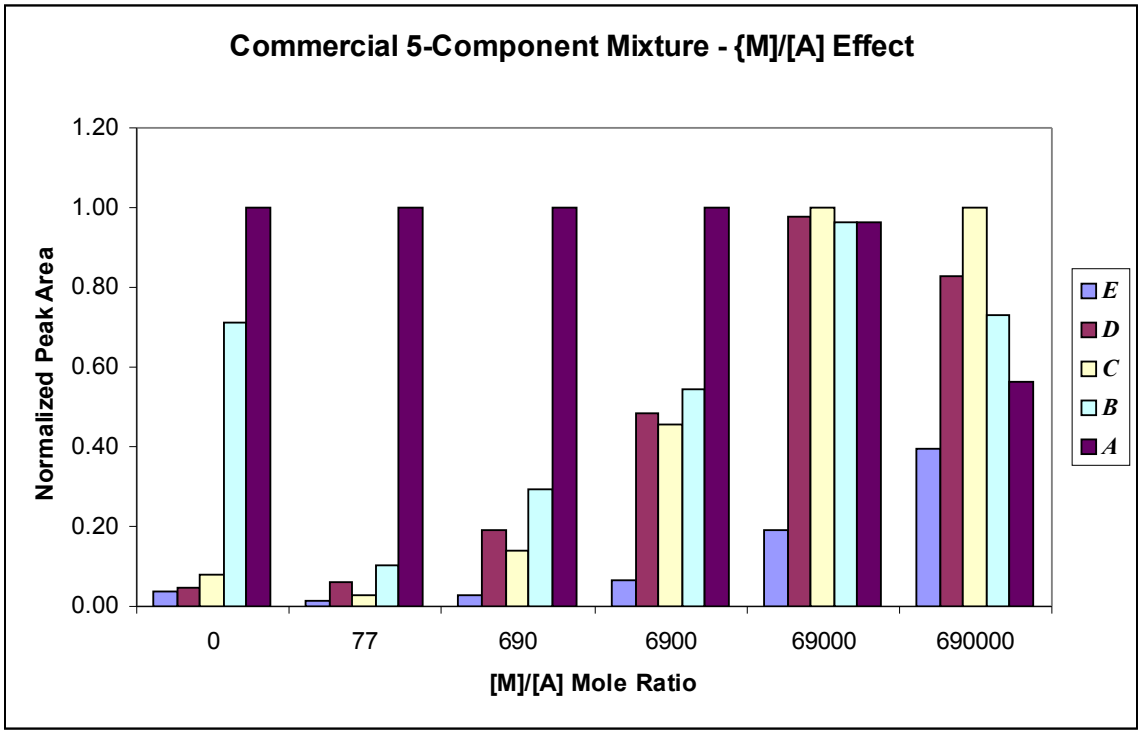

Figure 5. Normalized peak areas plotted vs M/A mole ratio (DCTB matrix) for the equimolar five-component mixture of Fig. 3. (See Figure 1 for analyte structures)

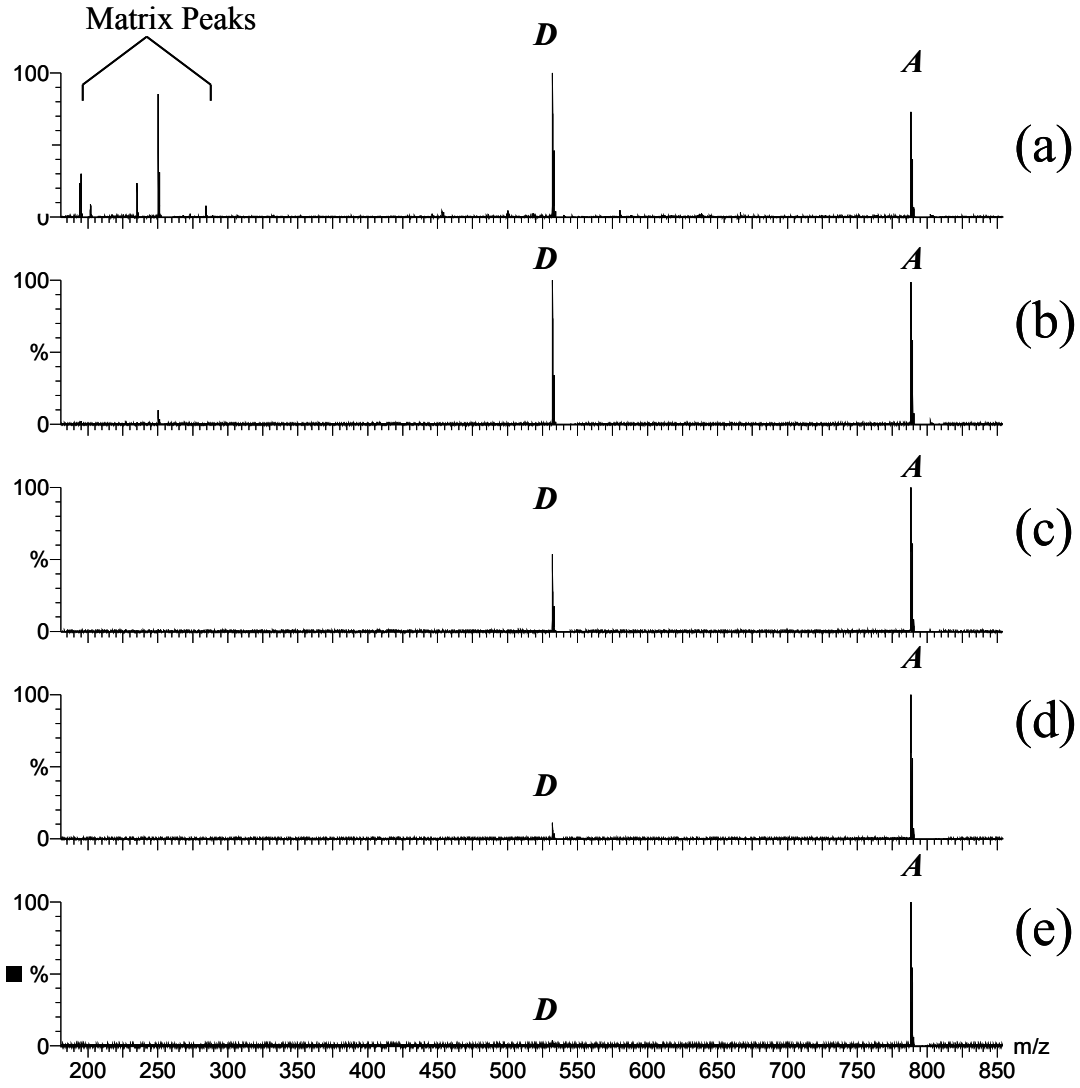

Figure 6. MALDI of equimolar mixture of analytes *A and D* in DCTB matrix, over a range of M/A mole ratio: a) M/A=660000, b) 66000, c) 6600, d) 660, and e) 73

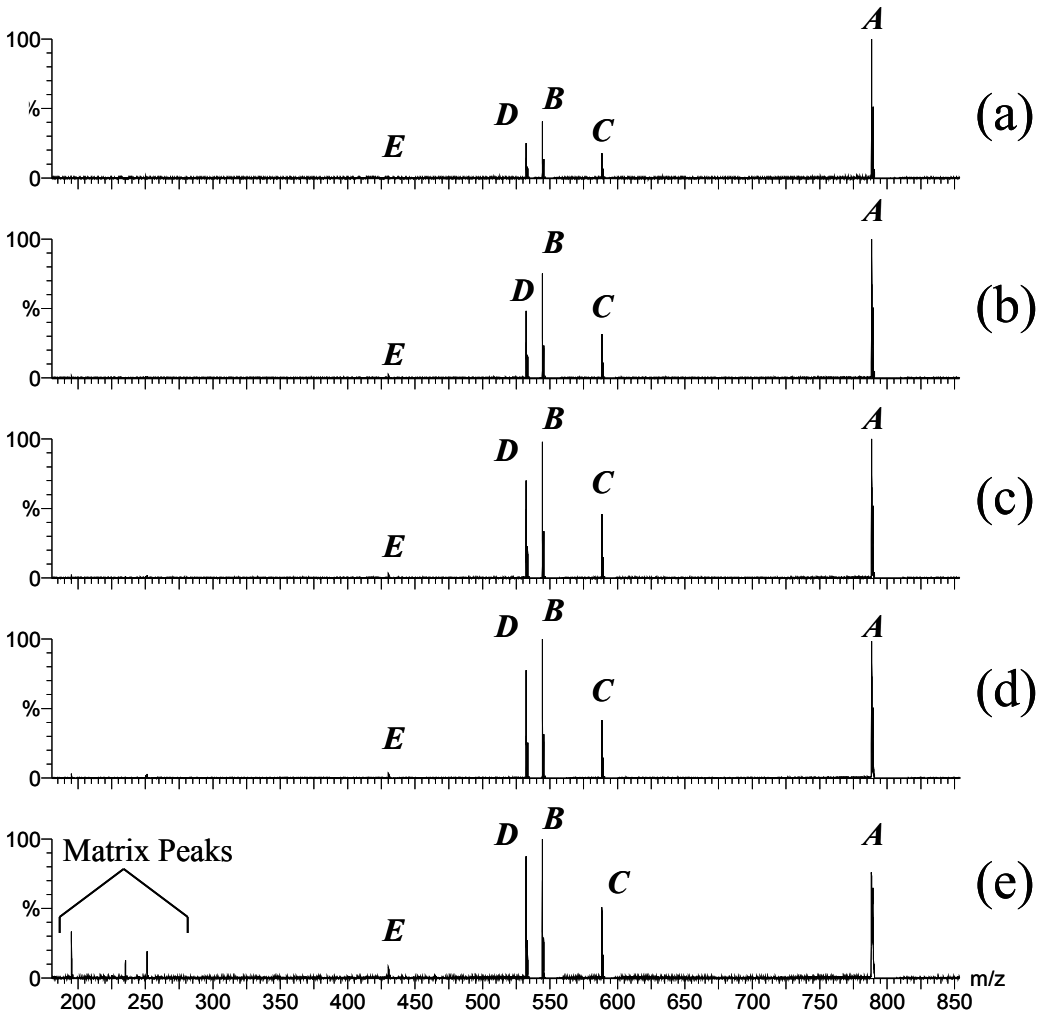

Figure 7. Laser power dependence of MALDI signal. The five component mixture of Fig. 3 was used. with DCTB as matrix at M/A = 690. Laser power in uJ/pulse: a) 5, b) 6, c) 7, d) 8, and e) 12.

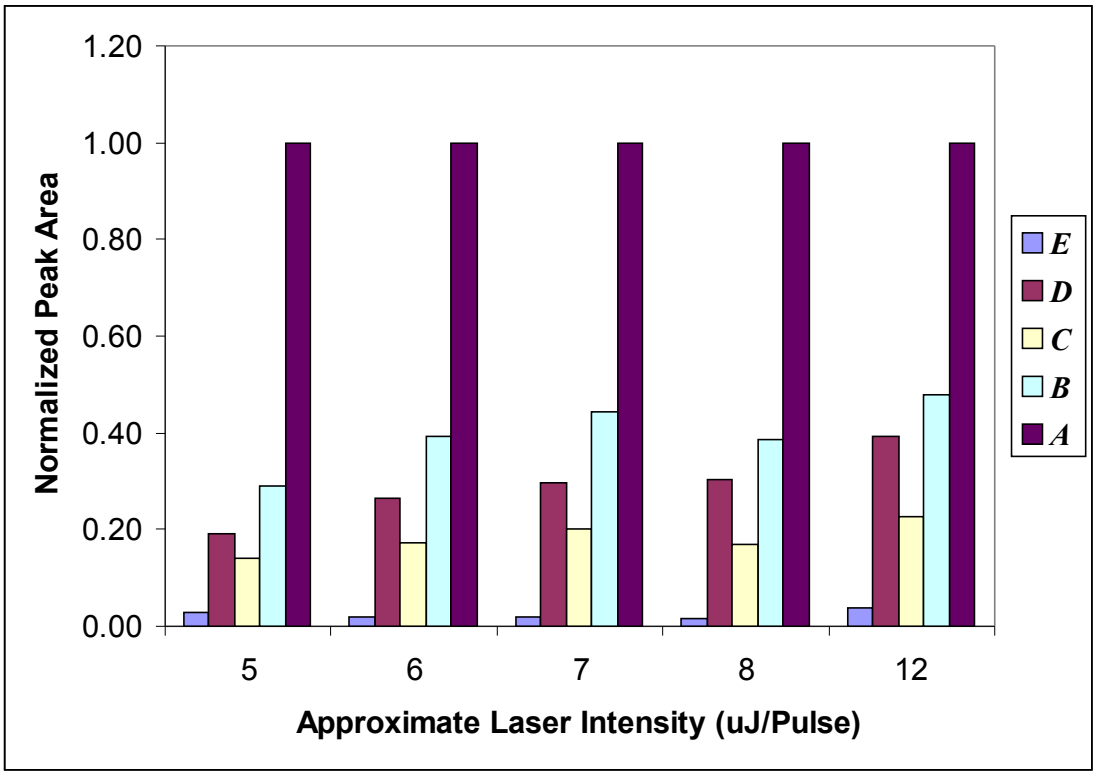

Figure 8. Laser power dependence of the integrated MALDI peak areas of Fig. 6.

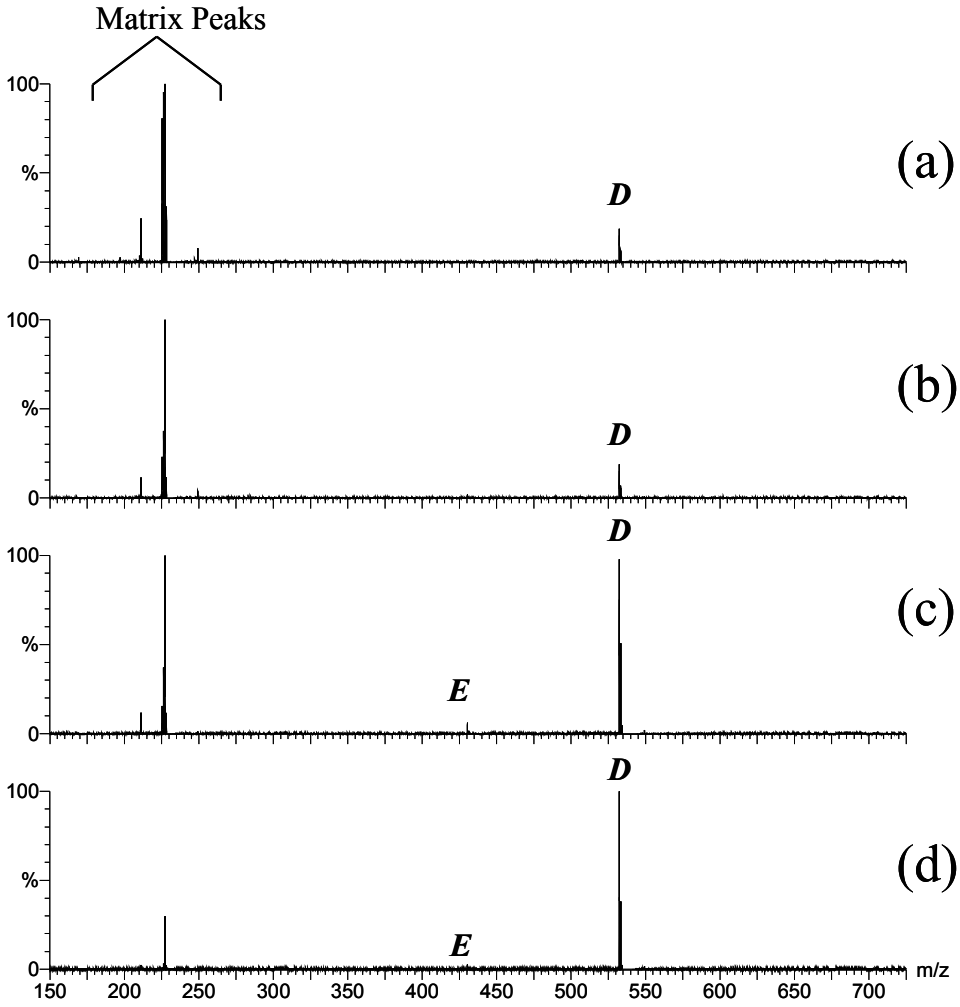

Figure 9. Equimolar mixture of rubrene (*D*) and D2NA (*E)* in dithranol matrix at M/A mole ratios of: a) M/A=65000, b) 6500, c) 650, and d) 70

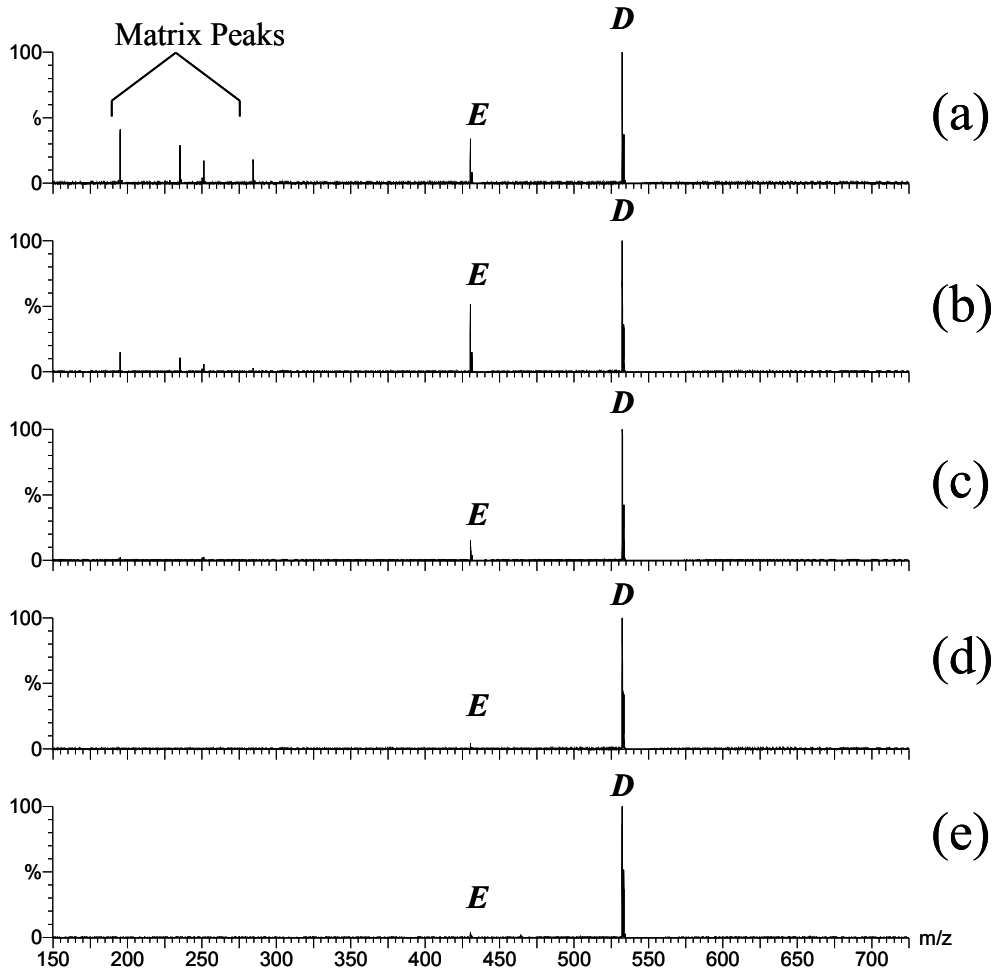

Figure 10. Equimolar mixture of analytes *D* and *E* using DCTB as the matrix, over a range of M/A mole ratio: a) M/A=53000, b) 5300, c) 530, d) 60, and e) 1

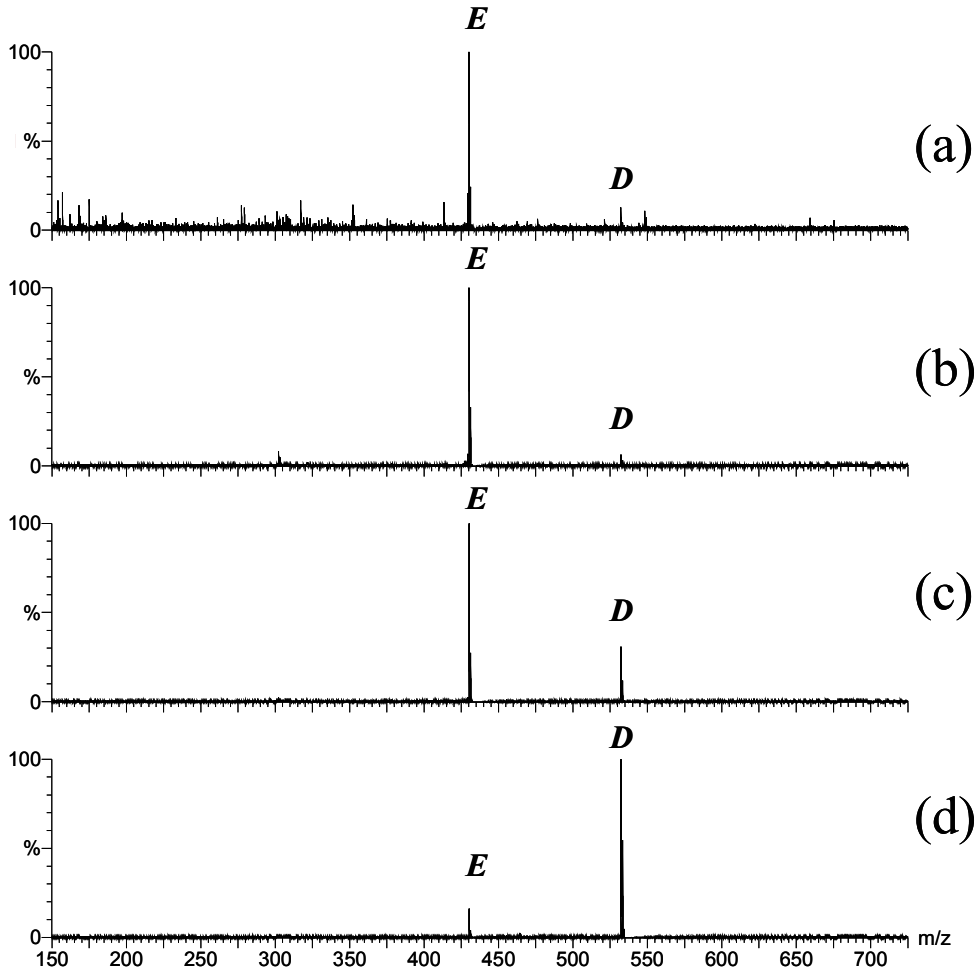

Figure 11. Equimolar mixture of rubrene (*D)* and D2NA (*E)* using nicotinic acid as the matrix with a range of M/A mole ratio: a) M/A=65000, b) 6500, c) 650, and d) 70